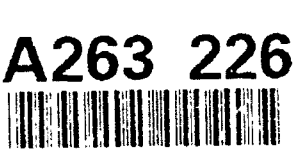

ARMY RESEARCH LABORATORY

Computation of Hypersonic Nosetip Heat Transfer Rates for an M829-Like Projectile

Bernard J. Guidos
Walter B. Sturek

ARL-MR-52 April 1993

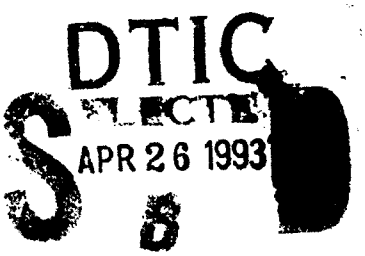

NOTICES

Destroy this report when it is no longer needed. DO NOT return it to the originator.

Additional copies of this report may be obtained from the National Technical Information Service, U.S. Department of Commerce, 5285 Port Royal Road, Springfield, VA 22161.

The findings of this report are not to be construed as an official Department of the Army position, unless so designated by other authorized documents.

The use of trade names or manufacturers' names in this report does not constitute indorsement of any commercial product.

REPORT DOCUMENTATION PAGE

Form Approved
OMB No. 0704-0188

1. AGENCY USE ONLY (Leave blank)	2. REPORT DATE	3. REPORT TYPE AND DATES COVERED
	April 1993	Final- January 1992-December 1992

4. TITLE AND SUBTITLE

COMPUTATION OF HYPERSONIC NOSETIP HEAT TRANSFER RATES FOR AN M829-LIKE PROJECTILE

5. FUNDING NUMBERS

1L162618AH80
62618A-00-001 J

6. AUTHOR(S)

BERNARD J. GUIDOS
WALTER B. STUREK

7. PERFORMING ORGANIZATION NAME(S) AND ADDRESS(ES)

U.S. Army Research Laboratory
ATTN: AMSRL-WT-PB
Aberdeen Proving Ground, MD 21005-5066

8. PERFORMING ORGANIZATION REPORT NUMBER

9. SPONSORING/MONITORING AGENCY NAME(S) AND ADDRESS(ES)

US Army Research Laboratory
ATTN: AMSRL-OP-CI-B (Tech Lib)
Aberdeen Proving Ground, Maryland 21005-5066

10. SPONSORING/MONITORING AGENCY REPORT NUMBER

ARL-MR-52

11. SUPPLEMENTARY NOTES

12a. DISTRIBUTION/AVAILABILITY STATEMENT

Approved for public release; distribution is unlimited.

12b. DISTRIBUTION CODE

13. ABSTRACT *(Maximum 200 words)*

Computational predictions are presented of in-flight blunt nosetip heat transfer rates for an M829-like projectile configuration. Predictions are made for higher-than-conventional flight velocities up to 3 km/sec (Mach 8.8), for both laminar and turbulent flows. Comparisons are made between two predictive approaches: (1) a time-dependent Navier-Stokes numerical technique and (2) a boundary-layer engineering analysis technique (known as ASCC). Additional comparison is made with wind-tunnel heat transfer measurements for a hemisphere-cylinder configuration at Mach 6.82. The Navier-Stokes predictions agree with the experimental data to within the estimated measurement accuracy. The comparisons between the two predictive approaches show agreement within 10% for laminar flow. For turbulent flow, the two codes agree within 10% at the stagnation point, and within about 30-40% further downstream. The heat transfer rates presented here provide a boundary condition model for subsequent analysis of projectile transient thermal response.

14. SUBJECT TERMS		15. NUMBER OF PAGES
Computational Fluid Dynamics	Blunt Body	24
Unsteady Navier-Stokes	Convection Heat Transfer	16. PRICE CODE
Supersonic Wind Tunnels	Aerodynamic Heating	

17. SECURITY CLASSIFICATION OF REPORT	18. SECURITY CLASSIFICATION OF THIS PAGE	19. SECURITY CLASSIFICATION OF ABSTRACT	20. LIMITATION OF ABSTRACT
UNCLASSIFIED	UNCLASSIFIED	UNCLASSIFIED	UL

INTENTIONALLY LEFT BLANK.

TABLE OF CONTENTS

INTENTIONALLY LEFT BLANK.

LIST OF FIGURES

INTENTIONALLY LEFT BLANK.

1. INTRODUCTION

The in-flight nosetip temperature response of kinetic energy (KE) projectiles is of significant interest to the U.S. Army. The design of a new class of hypersonic KE projectiles will partially depend upon a knowledge of the transient thermal response due to free-flight aerodynamic heating. The Aerodynamics Branch of the Weapons Technology Directorate, Army Research Laboratory is developing and maintaining a capability to accurately model the heating response of KE projectiles. A major area of focus is the blunt nosetip heating problem; in particular, the modeling of aerodynamic surface heat transfer characteristics.

This report documents recent computational predictions of nosetip heat transfer rates for an M829-like projectile configuration. The M829 projectile is currently launched from a 120mm gun at a velocity of about 1.7 km/sec (about Mach 4.9) at sea-level conditions. The M829 configuration is serving as one starting point for the design of hypersonic projectile configurations to be launched at still higher velocities. The heat transfer results presented here provide a model for boundary conditions in a separate analysis of the projectile unsteady thermal response.

The computational predictions are made for free-stream velocities up to 3 km/sec (Mach 8.8), using two different computational approaches. The first is a perfect gas, time-dependent, Navier-Stokes (N-S) finite-difference computational technique. The second is a boundary-layer engineering technique, known as the ABRES Shape Change Code (ASCC). Comparison is made between the results of these two approaches for laminar and turbulent flow conditions. As a basis for experimental validation, comparison is also made with wind-tunnel heat transfer measurements for a hemisphere-cylinder configuration at Mach 6.82.

2. BACKGROUND REMARKS

Designer concerns about KE projectile nosetip ablation have recently intensified due to the current interest in hypersonic launch technology. A major opportunity exists to apply and extend in-house computational fluid dynamics (CFD) capabilities in order to impact the design of the new class of hypervelocity projectiles.

The complete methodology involves two major aspects to be addressed. First, the in-flight surface heat transfer characteristics must be determined through a consideration of the projectile flowfield. Then, using a model which incorporates the heat transfer characteristics, the in-depth transient thermal response is determined by considering a heat conduction analysis within the projectile body. The long-standing approach is to consider these two

aspects of the problem separately. This report specifically addresses the first aspect only, focusing on the heat transfer characteristics of the blunt projectile nosetip.

Among the important issues to consider in the study of aerodynamic heat transfer is the determination of boundary-layer transition. Criteria exist for estimating the location and extent of the transition region, but the approach adopted here is to compute the fully laminar and fully turbulent flow cases separately. The laminar and turbulent cases basically represent the lower and upper bounds, respectively, of heating which would be expected to occur in actual flight.

Although the Navier-Stokes computational technique discussed herein assumes perfect gas behavior, it is emphasized that in-house work is ongoing to assess the importance of real gas effects on the heat transfer characteristics for the conditions of interest to the Army. The perfect gas results presented here will serve as a benchmark with which to compare and validate future CFD codes having perfect gas and real gas capabilities.

3. COMPUTATIONAL PREDICTIVE APPROACHES

Predictions of heat transfer characteristics are made using two different computational approaches. The first is a Navier-Stokes numerical technique; the second is an engineering technique known as ASCC. Comparison is made between the results of these two approaches in order to provide a benchmark for future applications. The ASCC code is attractive because it executes quickly on a typical workstation or mini-computer. Navier-Stokes technology, however, is required for more complex problems, such as those involving (1) non-axisymmetric shapes, (2) flat nosetip shapes, or (3) three-dimensional effects due to angle-of-attack or geometric irregularities.

3.1 Unsteady Navier-Stokes Technique (N-S). Surface heat transfer characteristics were computed using an unsteady (i.e., time-dependent) Navier-Stokes (N-S) computational technique on a Cray X-MP/48 supercomputer located at Aberdeen Proving Ground. This technique, as reported by Pulliam and Steger (1980) and Kutler, Pulliam, et al (1980), is a three-dimensional, finite-difference, viscous flow solution procedure for compressible flow fields. The N-S technique temporally integrates the dimensionless, transformed, time-dependent, thin-layer, mass-averaged Navier-Stokes equations in strong conservation law form, for a perfect gas. The solution vector, $\bar{Q}$, is

$$\bar{Q} = (\rho, \rho u, \rho v, \rho w, e) \tag{1}$$

where the density is ρ; the Cartesian velocity components are u, v, and w; and the total energy per unit volume is e. The solution vector is obtained at each grid point by integrating toward a steady state. Currently, a set of inviscid, viscous laminar, and viscous turbulent axisymmetric flow solutions at a single Mach number takes on the order of an hour of CPU time to generate on a Cray X-MP using a 50 x 65 grid. Efforts are continuing in-house to reduce the time requirements further, but are not a topic for discussion in this report.

This Navier-Stokes technique has been applied and validated in-house (Sturek, Guidos, et al 1983; Guidos, Weinacht, Dolling 1990) for blunt nosetip configurations. A range of comparisons has been made in the references between N-S results and measured surface pressures, aerodynamic forces, velocity profiles, and skin friction coefficient. Details of the technique, including the governing equations and numerical algorithm, can be traced through the aforementioned references.

The local vector of surface heat transfer rate per unit area, $\bar{q}$, is obtained from the computed flowfield solutions using Fourier's Law, i.e:

$$\bar{q} = -\kappa(\frac{\partial T}{\partial \bar{n}}) \mid_{wall} \tag{2}$$

where κ is the coefficient of conductivity of the fluid and $\bar{n}$ is the physical coordinate perpendicular to the surface. The vector $\bar{q}$ is obtained from the computed flowfields using a first-order, one-sided, finite-difference approximation along the transformed coordinate which extends outward from the wall. The local heat transfer rate from the fluid to the body per unit area, q, is then defined as:

$$q = -\bar{n} \cdot \bar{q} \tag{3}$$

3.2 Boundary-Layer Engineering Technique (ASCC). Surface heat transfer characteristics were also computed using an axisymmetric boundary-layer engineering technique known as the ABRES Shape Change Code - ASCC (Suchsland 1980). The ASCC code utilizes a modified Newtonian surface pressure distribution and inviscid flowfield approximations to generate boundary-layer edge flow conditions.

The ASCC code is of special interest because it generates adiabatic wall temperatures and heat transfer coefficients in less than a minute of CPU time on a typical workstation or mini-computer. Such quickness makes it a popular tool in aeroballistics design. Comparison of ASCC results with Navier-Stokes results at sea-level atmospheric flight conditions is an important step in establishing a benchmark for future applications of both codes.

4. RESULTS

4.1 Hemisphere-Cylinder Wind-Tunnel Case. Hypersonic surface heat transfer rate measurements for a hemisphere-cylinder wind-tunnel model are documented in a report by Crawford and McCauley (1956). The configuration is a thin-walled hemisphere-cylinder of diameter 76.84 mm, shown in Figure 1. Nominal free-stream conditions are given as: Mach number, M_∞=6.82; Reynolds number based on body diameter, Re_d=1.03×10^6 and 3.4×10^5; static temperature, T_∞=59 K, and total temperature, T_o=611 K. Real gas effects in this experiment are expected to be negligible, since the total temperature is significantly below the threshold which excites the vibrational modes of O_2 or N_2. The flow is reported to be laminar, and the computational results are presented here assuming fully laminar flow conditions.

In the experiment, the surface temperature distribution on the model was measured using an array of thermocouples. Thermocouple readings were recorded during each run every 3 seconds as the model temperature increased. The local heat transfer rate, q, at each thermocouple location was determined through an analysis which is described in the above referenced report. In the report, the measured heat transfer rates were then plotted as a function of the local wall temperature, T_w. Then, using the assumption that q is linear with respect to T_w, linear fits were determined and plotted. The differences in the measured and fitted values of heat transfer rates as reported suggest a measurement uncertainty on the order ±15%.

The Navier-Stokes computations were performed by prescribing a wall temperature which, unlike that of the experiment, is constant with respect to both time and body location. The lowest temperature where the measured values of heat transfer rates (in addition to the fitted values) are reported at all thermocouple locations and for all Reynolds numbers is T_w=385 K (about 63% of the nominal free-stream total temperature). This is the wall temperature prescribed in the computational results to be presented.

Figure 2 shows the comparison of computed and measured heat transfer rates plotted as a function of axial location for the case Re_d=1.03×10^6. At the stagnation point (x/r_n=0.0), the computed heat transfer rate is about 5% higher than the measured value. At x/r_n=0.5 and x/r_n=1.0 , the computed values are about 15% lower than the measured values.

Figure 3 shows the comparison for the case Re_d=3.4×10^5. The heat transfer rates at this Reynolds number are about 60% of the heat transfer rates of the previous figure. The computed stagnation point heat transfer rate is about 10% higher than the measured value. At x/r_n=0.5, the computed value is about 15% higher than the measured value; at x/r_n=1.0,

the computed value is about 10% lower than the measured value. The comparisons of heat transfer rate shown in Figures 2 and 3 appear to be within the uncertainty of the measured data, and serve to validate the Navier-Stokes computational analysis for these conditions.

4.2 M829-Like Configuration Free-Flight Case. The M829 projectile configuration, Figure 4, is currently serving as one starting point for the design of new hypersonic configurations. The reference diameter is that of the cylinder, 27.05 mm. The standard nosetip geometry, Figure 5, is assumed to be a spherical cap of radius 1.65 mm tangent to an 8° cone. Flight conditions are taken to be standard, atmospheric, sea-level conditions. Results are shown for free-stream velocities of 1.7, 2.0, 2.5, and 3.0 km/sec; the corresponding Reynolds numbers based on the reference diameter are 3.00×10^6, 3.62×10^6, 4.53×10^6, and 5.40×10^6, respectively. The angle-of-attack is 0°; the wall temperature and free-stream temperature are both 293 K.

Figures 6 through 9 show the computed surface heat transfer rates for velocities of 1.7, 2.0, 2.5, and 3.0 km/sec, respectively. The N-S and ASCC solutions are compared for laminar and turbulent flow conditions. The laminar stagnation point heat transfer rates compare with a maximum disagreement of about 5%. Downstream, the comparison is improved to within 2%. The turbulent stagnation point heat transfer rates compare to within about 5%. The N-S results show the maximum turbulent heat transfer rates to be up to 40% higher than the ASCC results. Further downstream, disagreement is also as high as 40%.

Both codes show the maximum turbulent heat transfer rate to occur downstream of the stagnation point, in the range $0.1 \leq x/r_n \leq 0.15$ (about 25°-30° off-axis). At each velocity, the ASCC results predict the same value of stagnation point heat transfer for the laminar and turbulent cases. The Navier-Stokes results, however, predict a turbulent stagnation point heat transfer rate about 10% higher than the laminar rate. In all cases, the turbulent ASCC prediction is bounded by the turbulent N-S prediction and the two laminar predictions.

Figure 10 shows predictions of laminar heat transfer rate at 2.5 km/sec for two additional nosetip radii other than the standard 1.65 mm (0.065 in), specifically 0.762 mm (.03 in) and 2.54 mm (0.1 in). In both cases, the laminar stagnation point heat transfer rates between the two codes agree to within 5%. Agreement over the remaining spherical portions is around 10%, and agreement on the cone portions is within 1%. Compared to the standard nosetip, the larger (2.54 mm radius) nosetip decreases the laminar stagnation point heat transfer rate by about 20%. The smaller (0.762 radius) nosetip increases the laminar stagnation point heat transfer rate by about 35%.

Figure 11 shows the comparison of turbulent heat transfer rate for the two additional

nosetip radii. The relative comparisons between the two codes are similar to those of the standard nosetip. The turbulent stagnation point heat transfer rates compare to within about 10%. The N-S results show the maximum turbulent heat transfer rates to be about 40% higher than the ASCC results. Compared to the standard nosetip, the larger nosetip decreases the turbulent stagnation point heat transfer rate by about 20%, and by about 15% at the maximum heating point. The smaller nosetip increases the turbulent stagnation point heat transfer rate by about 40%, and by about 30% at the maximum heating point.

5. CONCLUSION

Computational predictions have been presented of heat transfer characteristics for the sphere-cone nosetip of an M829-like projectile configuration. Results were presented for velocities in the range 1.7 to 3.0 km/sec, laminar and turbulent flow conditions. Comparisons were made between two computational techniques: (1) a time-dependent Navier-Stokes technique and (2) the ABRES Shape Change Code boundary-layer technique.

Comparisons of laminar nosetip heat transfer rate between the two codes showed agreement within 5% at the stagnation point, and within 2% further downstream. Comparisons of turbulent heat transfer rates between the two codes showed notable disagreement. The N-S approach predicted a 10% higher turbulent heat transfer rate than ASCC at the stagnation point, and up to 40% higher turbulent heat transfer rate at the point of maximum heat transfer rate and downstream. Both codes showed the location of maximum turbulent heat transfer rate to occur about 25°-30° off-axis.

At each velocity, the ASCC turbulent heat transfer rate was bounded by the N-S turbulent heat transfer rate and the two laminar rates. Furthermore, results for two additional nosetip radii at 2.5 km/sec showed comparisons which were similar to the standard nosetip radius.

Comparison was also made between Navier-Stokes results and existing wind-tunnel laminar heat transfer rate measurements for a hemisphere-cylinder model at Mach 6.82. The Navier-Stokes results at two different Reynolds numbers compared with the measured values by about 5%-10% at the stagnation point and within 10%-15% elsewhere. The estimated uncertainty of the measured values is about $\pm 15\%$.

The heat transfer characteristics which have been presented here provide a necessary boundary condition for subsequent in-depth transient thermal analysis of M829-like projectile configurations. The Navier-Stokes and ASCC techniques will continue to be utilized to generate heat transfer characteristics for prospective designs. Additionally, the results presented here will serve as a benchmark for CFD codes having real gas capabilities.

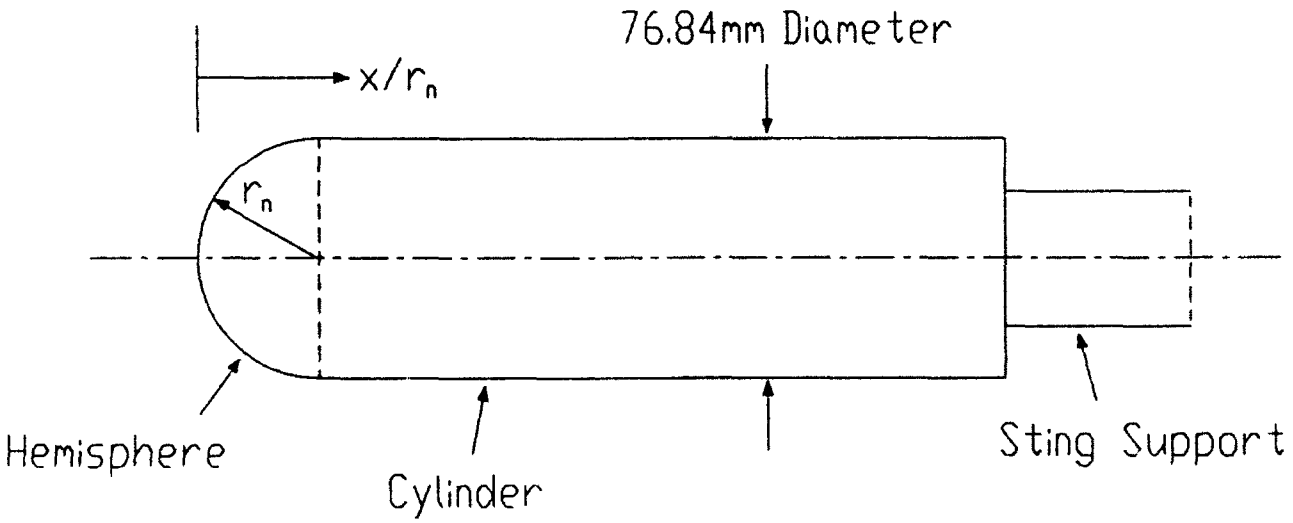

Figure 1. Illustration of Hemispher-Cylinder Wind-Tunnel Model

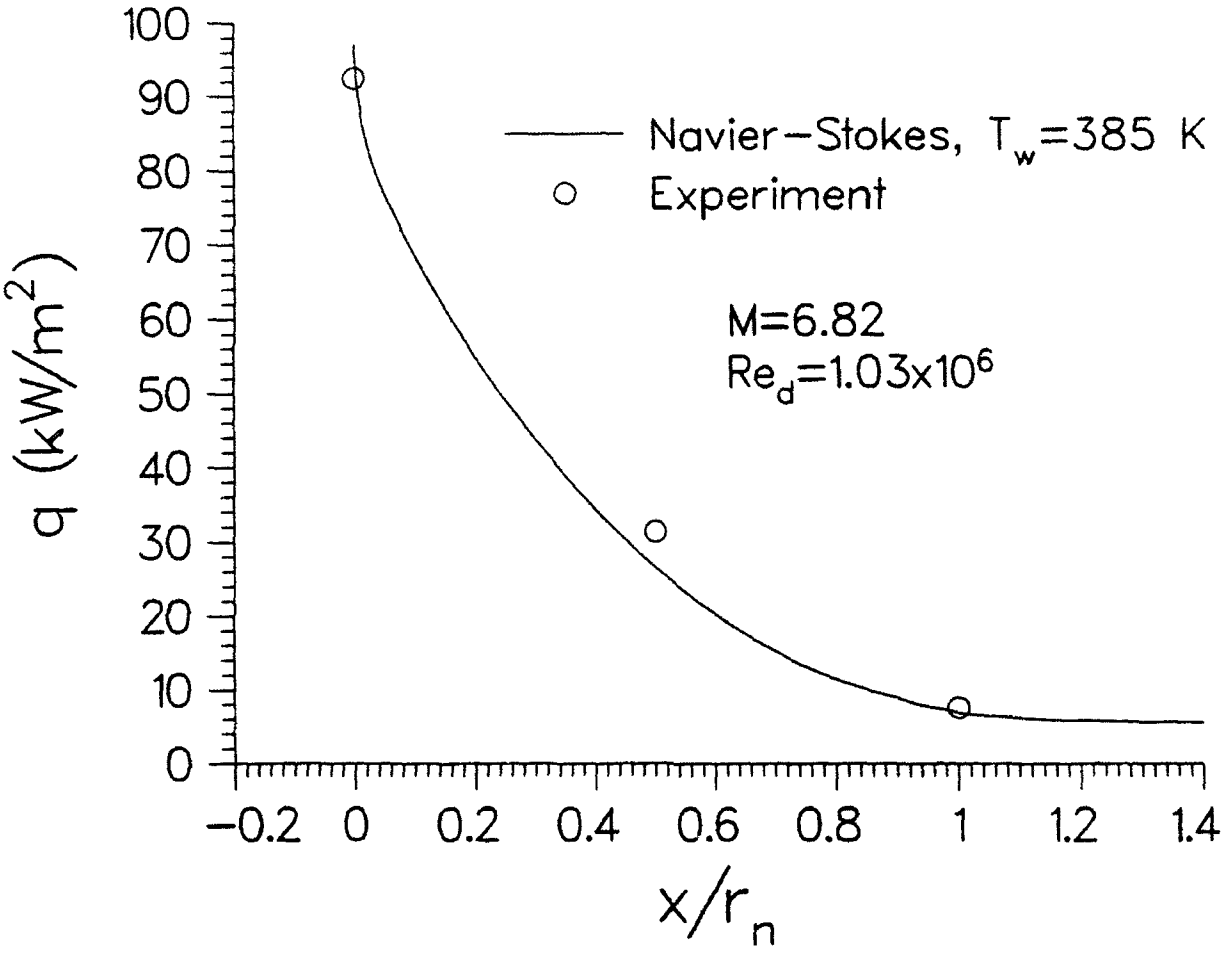

Figure 2. Heat Transfer Rate, Hemisphere-Cylinder Wind-Tunnel Model, M=6.82, Re_d = 1.03 × 10^6

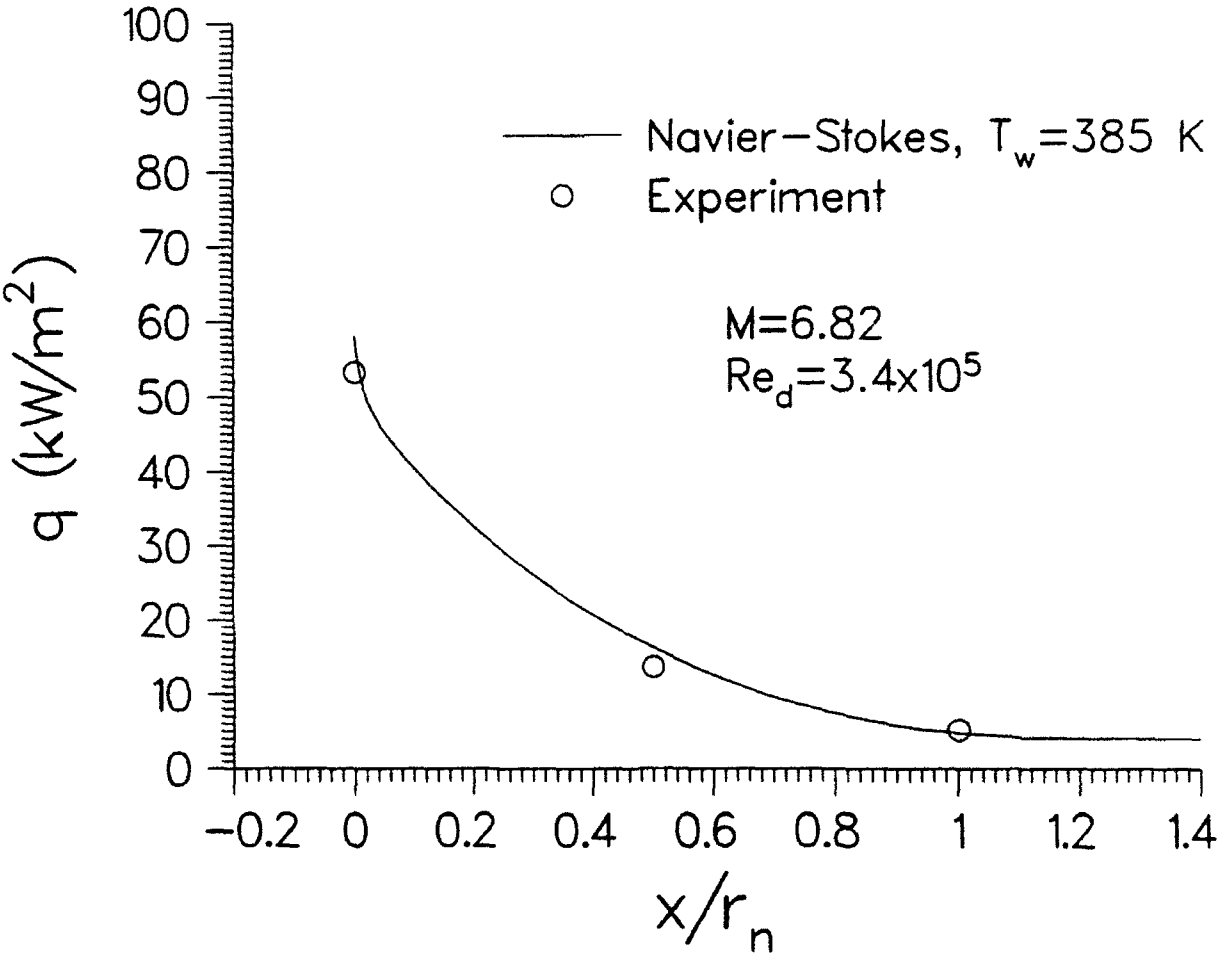

Figure 3. Heat Transfer Rate, Hemisphere-Cylinder Wind-Tunnel Model, M=6.82, Re_d = 3.4 × 10^5

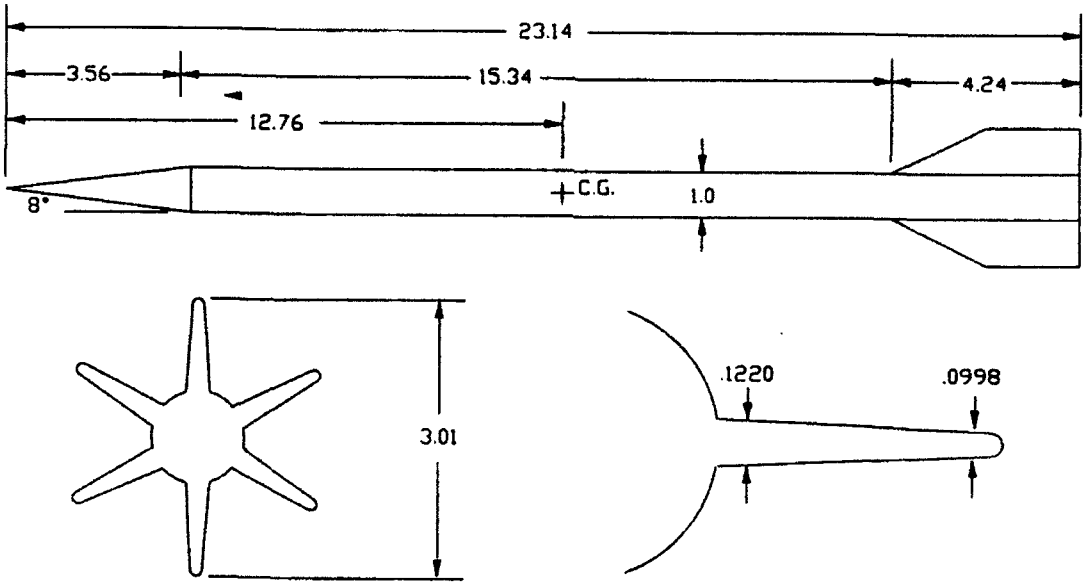

Figure 4. Illustration of M829 Projectile

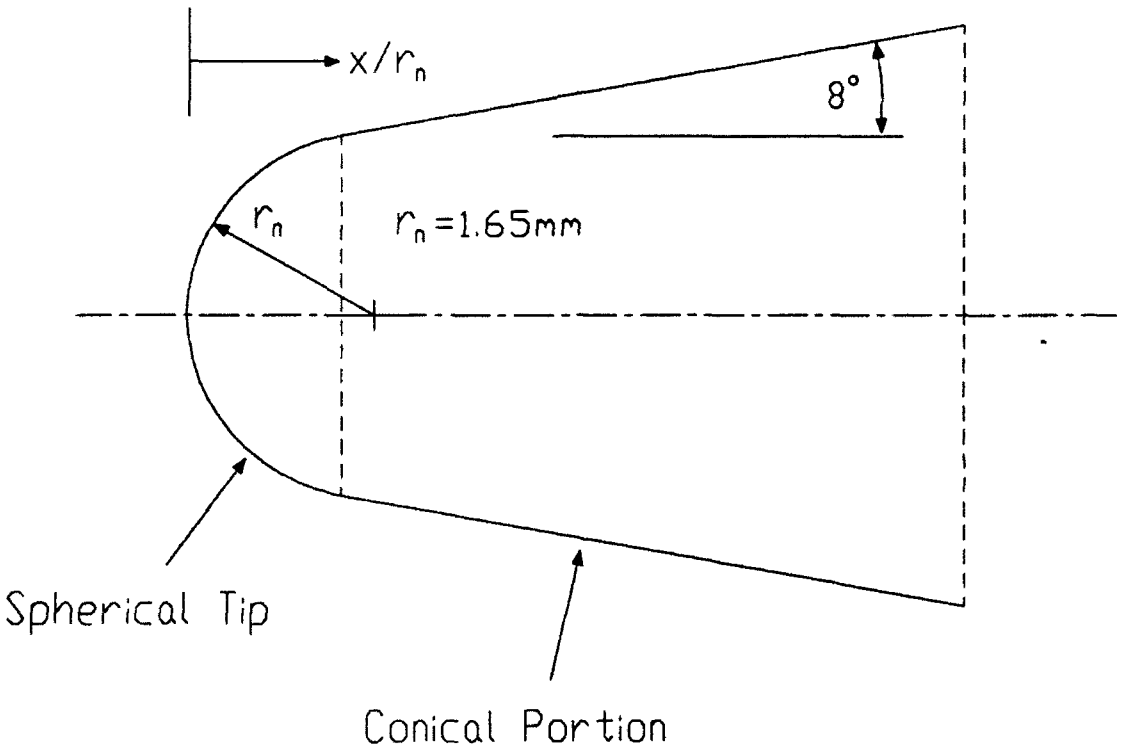

Figure 5. Illustration of M829-Like Nosetip

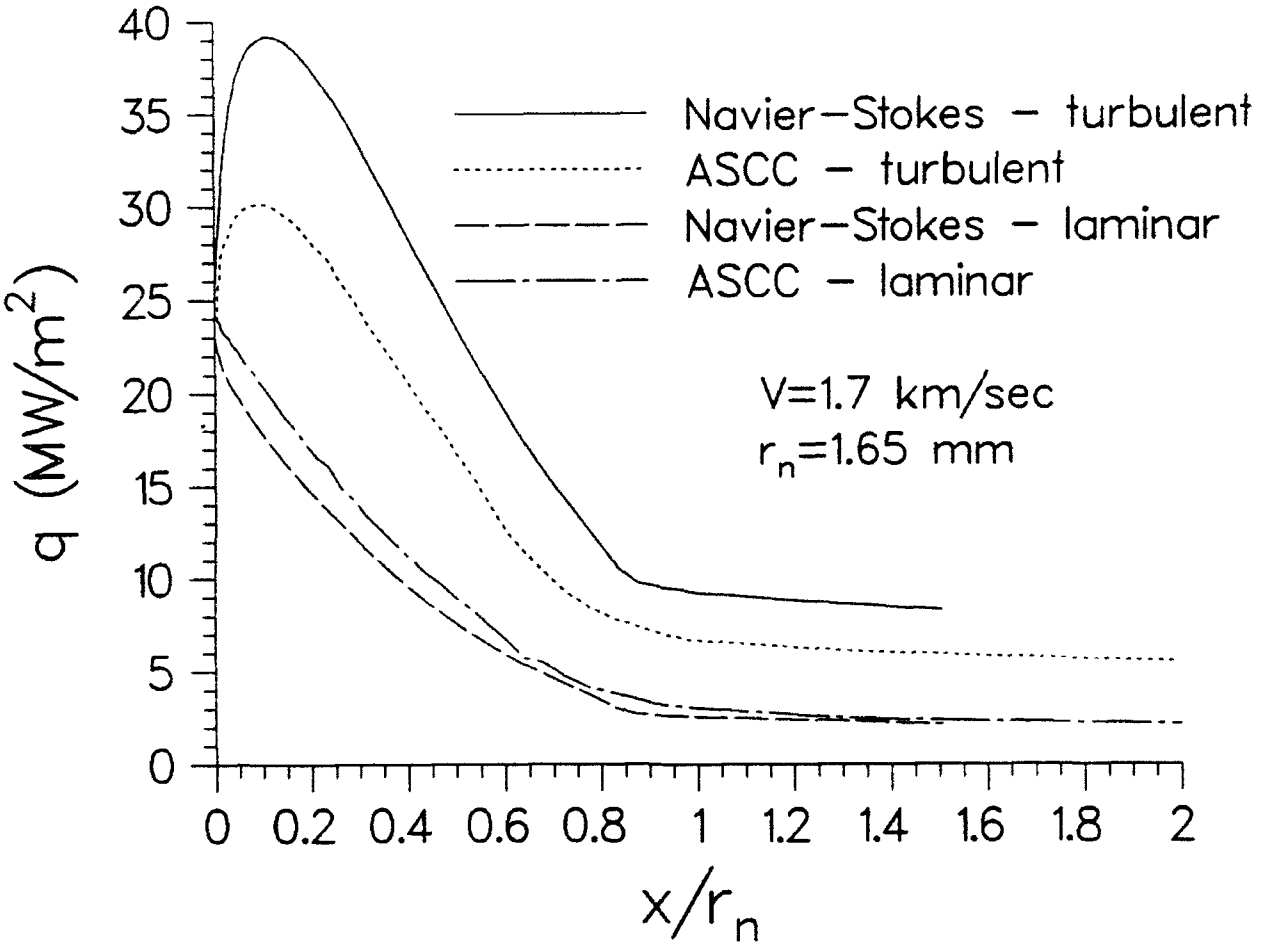

Figure 6. Heat Transfer Rate, M829-Like Nosetip, 1.7 km/sec

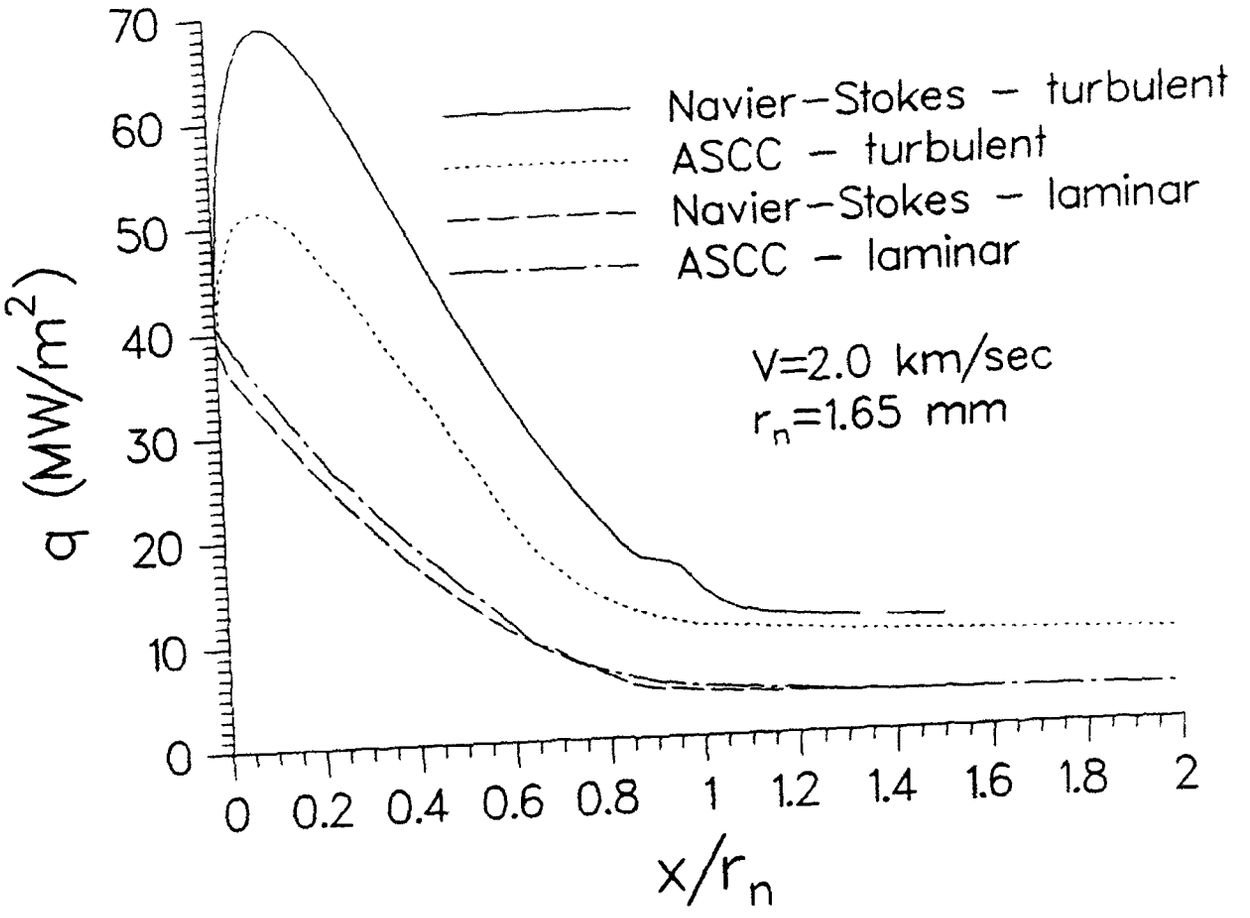

Figure 7. Heat Transfer Rate, M829-Like Nosetip, 2.0 km/sec

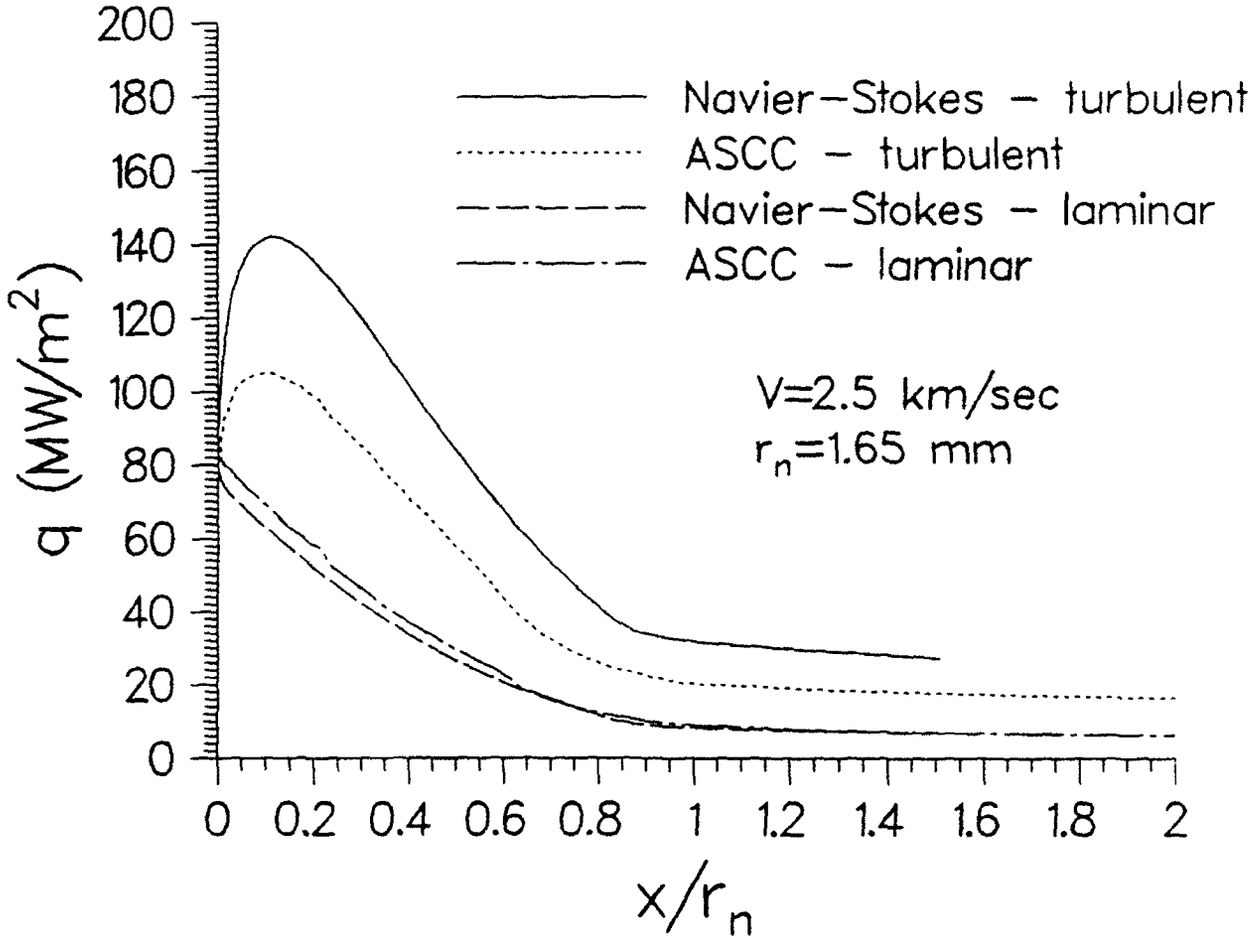

Figure 8. Heat Transfer Rate, M829-Like Nosetip, 2.5 km/sec

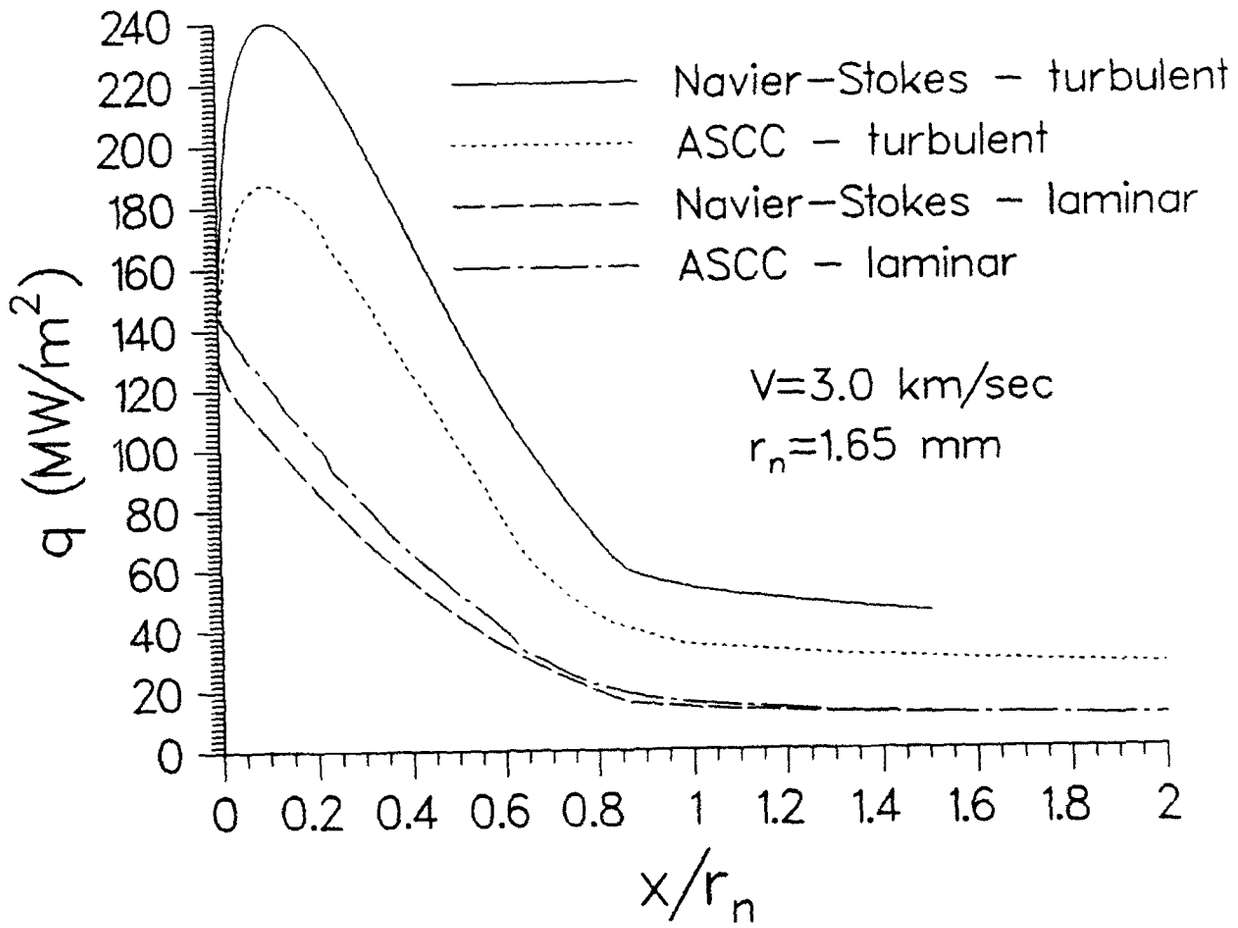

Figure 9. Heat Transfer Rate, M829-Like Nosetip, 3.0 km/sec

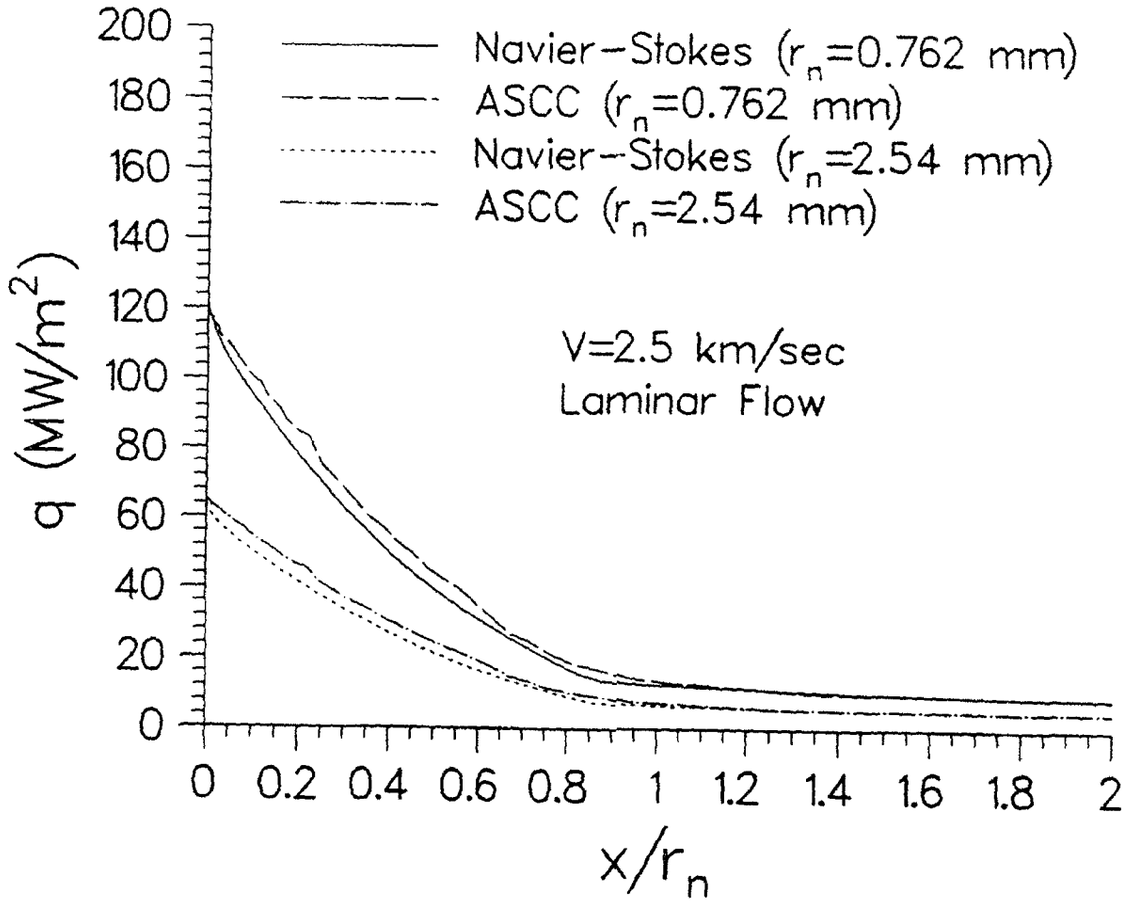

Figure 10. Heat Transfer Rate, 2 Alternate Nosetips, Laminar Flow, 2.5 km/sec

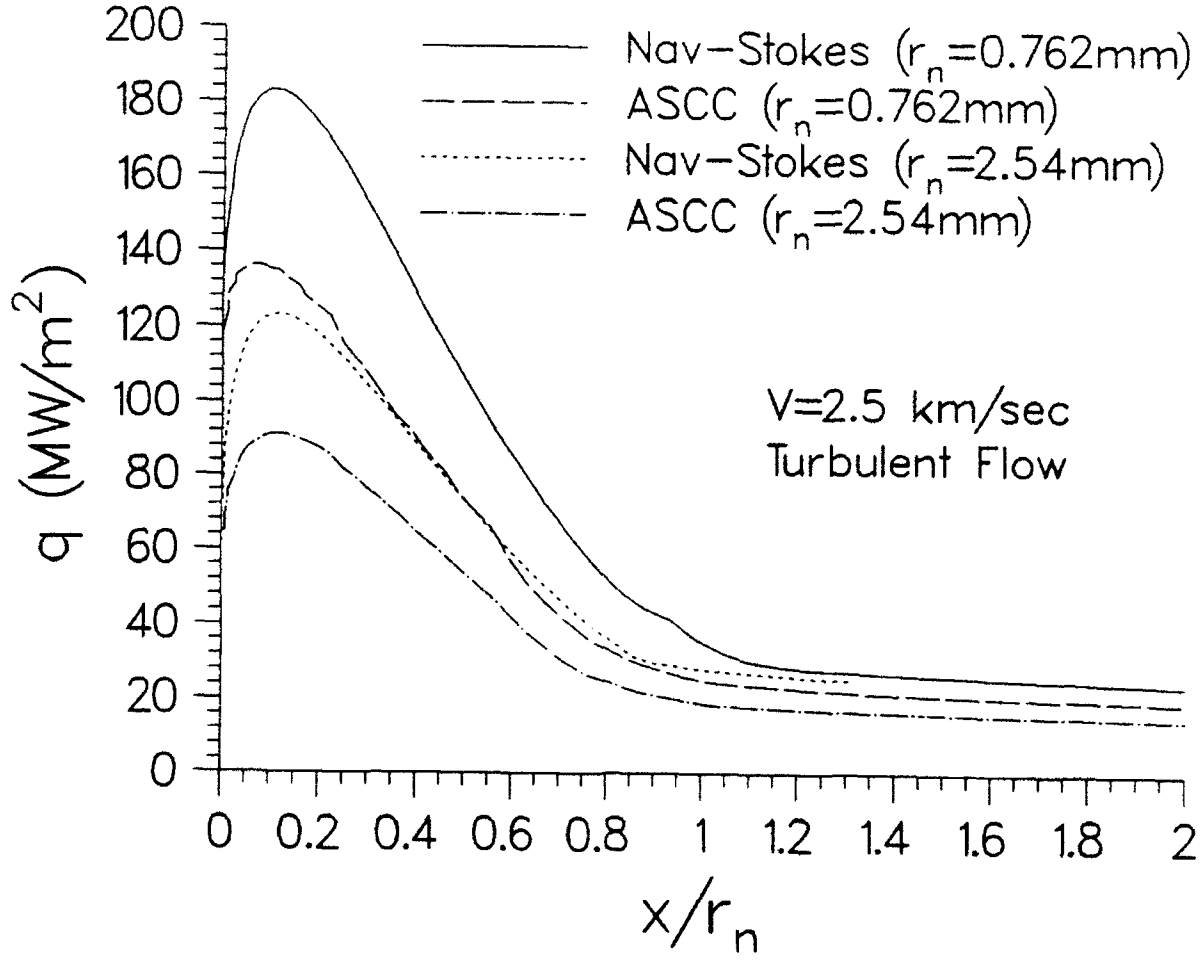

Figure 11. Heat Transfer Rate, 2 Alternate Nosetips, Turbulent Flow, 2.5 km/sec

INTENTIONALLY LEFT BLANK.

6. REFERENCES

Crawford, D.H. and W.D. McCauley, "Investigation of the Laminar Aerodynamic Heat-Transfer Characteristics of a Hemisphere-Cylinder in the Langley 11-inch Hypersonic Tunnel at a Mach Number of 6.8." NACA Technical Note 3706, July 1956.

Guidos, B.J., P. Weinacht, and D.S. Dolling, "Comparison of Navier-Stokes Computation and Experiment for Pointed, Spherical, and Flat Tipped Shell at Mach 2.95." U.S. Army Ballistic Research Laboratory, BRL-TR-3076, January 1990. (AD A218749)

Kutler, P., J.A. Pedalty, and T.H. Pulliam, "Supersonic Flow over Three-Dimensional Ablated Nosetips using an Unsteady Implicit Numerical Procedure." AIAA Paper No. 80-0063, January 1980.

Pulliam, T.H. and J.L. Steger, "Implicit Finite-Difference Simulations of Three-Dimensional Compressible Flow." AIAA Journal, Vol. 18, No. 2, February 1980, pp. 159-167.

Sturek, W.B., D.C. Mylin, B.J. Guidos, and C.J. Nietubicz, "Navier-Stokes Computational Study of the Influence of Shell Geometry on the Magnus Effect at Supersonic Speeds." U.S. Army Ballistic Research Laboratory, ARBRL-TR-02501, June 1983. (AD A130630)

Suchsland, K.E., "Aerothermal Assessment of Projectiles Using the ABRES Shape Change Code (ASCC)." ACUREX Report TM-80-31/AS, July 1980.

INTENTIONALLY LEFT BLANK.

LIST OF SYMBOLS

d	reference diameter
e	total energy per unit volume
M	Mach number
$\bar{n}$	physical coordinate normal to the wall
$\bar{Q}$	Vector of dependent variables in Navier-Stokes technique
$\bar{q}$	vector of heat transfer rate per unit area in $\bar{n}$ direction
q	heat transfer rate from fluid to body per unit area
Re_d	free-stream Reynolds number based on reference diameter
r_n	nosetip radius
T	temperature
u, v, w	Cartesian velocity components
V	free-stream velocity
x	axial distance from projectile nosetip

Greek Symbols

κ	coefficient of thermal conductivity
ρ	density

Subscripts

w	wall condition
o	total condition
∞	free-stream condition

INTENTIONALLY LEFT BLANK.

No. of Copies	Organization
2	Administrator Defense Technical Info Center ATTN: DTIC-DDA Cameron Station Alexandria, VA 22304-6145
1	Commander U.S. Army Materiel Command ATTN: AMCAM 5001 Eisenhower Ave. Alexandria, VA 22333-0001
1	Director U.S. Army Research Laboratory ATTN: AMSRL-OP-CI-AD, Tech Publishing 2800 Powder Mill Rd. Adelphi, MD 20783-1145
2	Commander U.S. Army Armament Research, Development, and Engineering Center ATTN: SMCAR-IMI-I Picatinny Arsenal, NJ 07806-5000
2	Commander U.S. Army Armament Research, Development, and Engineering Center ATTN: SMCAR-TDC Picatinny Arsenal, NJ 07806-5000
1	Director Benet Weapons Laboratory U.S. Army Armament Research, Development, and Engineering Center ATTN: SMCAR-CCB-TL Watervliet, NY 12189-4050
(Unclass. only) 1	Commander U.S. Army Rock Island Arsenal ATTN: SMCRI-IMC-RT/Technical Library Rock Island, IL 61299-5000
1	Director U.S. Army Aviation Research and Technology Activity ATTN: SAVRT-R (Library) M/S 219-3 Ames Research Center Moffett Field, CA 94035-1000

No. of Copies	Organization
1	Commander U.S. Army Missile Command ATTN: AMSMI-RD-CS-R (DOC) Redstone Arsenal, AL 35898-5010
1	Commander U.S. Army Tank-Automotive Command ATTN: ASQNC-TAC-DIT (Technical Information Center) Warren, MI 48397-5000
1	Director U.S. Army TRADOC Analysis Command ATTN: ATRC-WSR White Sands Missile Range, NM 88002-5502
1	Commandant U.S. Army Field Artillery School ATTN: ATSF-CSI Ft. Sill, OK 73503-5000
(Class. only) 1	Commandant U.S. Army Infantry School ATTN: ATSH-CD (Security Mgr.) Fort Benning, GA 31905-5660
(Unclass. only) 1	Commandant U.S. Army Infantry School ATTN: ATSH-CD-CSO-OR Fort Benning, GA 31905-5660
1	WL/MNOI Eglin AFB, FL 32542-5000
	Aberdeen Proving Ground
2	Dir, USAMSAA ATTN: AMXSY-D AMXSY-MP, H. Cohen
1	Cdr, USATECOM ATTN: AMSTE-TC
1	Dir, ERDEC ATTN: SCBRD-RT
1	Cdr, CBDA ATTN: AMSCB-CI
1	Dir, USARL ATTN: AMSRL-SL-I
10	Dir, USARL ATTN: AMSRL-OP-CI-B (Tech Lib)

No. Copies | Organization

2 Institute for Advanced Technology
University of Texas at Austin
ATTN: W. Reinecke
T. Kiehne
4030-2 W. Braker Lane
Austin, TX 78759-5329

6 Commander
US Army Armament R&D Center
US Army AMCCOM
ATTN: R. Kline
S. Kahn
J. Grau
H. Hudgins
C. Ng
B. Wong
Picatinny Arsenal, NJ 07806-5001

2 Commander
Naval Surface Warfare Center
Applied Mathematics Branch
ATTN: Code R44 (F. Priolo)
Code R44 (A. Wardlaw)
White Oak Laboratory
Silver Spring, MD 20903-5000

1 Science and Technology Associates, Inc.
ATTN: A. Glasser
4001 N. Fairfax Drive - Suite 700
Arlington, VA 22203

1 Commander
US Army Armament R&D Center
US Army AMCCOM
SMCAR-CCH-V
ATTN: E. Fennell
Picatinny Arsenal, NJ 07806-5001